A direct method for the simultaneous estimation of self-steepening and the fractional Raman contribution in fiber optics

Nicolás Linale, Juan Bonetti, Pablo I. Fierens, *Senior Member, IEEE*, Santiago M. Hernandez, and Diego F. Grosz

***Abstract*—We propose an original, simple, and direct method for the simultaneous estimation of the self-steepening parameter and the fractional Raman contribution in fiber optics. Our proposal is based on the dependence of the modulation instability gain on both parameters, as obtained from a linear stability analysis of the newly introduced photon-conserving generalized nonlinear Schrödinger equation (pcGNLSE), and requires only the CW or quasi-CW pumping of the waveguide under test and a few direct spectral measurements. Further, we demonstrate the feasibility of the estimation procedure by means of detailed simulations for typical waveguide parameters in relevant spectral ranges. Last, we discuss the range of applicability of the proposed method and compare its results, advantages, and disadvantages with a recently introduced method based on short-pulse dynamics.**

***Index Terms*—Nonlinear optics, Raman scattering, self-steepening.**

I. Introduction

STIMULATED Raman scattering is a most relevant nonlinear phenomenon encountered in the context of short-pulse propagation in optical waveguides. It manifests as an energy transfer from high to low frequency components in the pulse spectrum and is responsible for the redshift of short pulses, an effect often referred to as the Raman-induced frequency shift (RIFS). This RIFS has been extensively studied in the context of solitons [1], [2] as well as the concomitant time shift enabled by the group-velocity dispersion (GVD) of the medium. Both frequency and time shifts have been widely observed in experiments [3], [4] and find applications in a vast number of areas in optics and photonics, such as in frequency-tunable femtosecond sources [5], signal processing, and tunable time delays [6], to name a few.

Another most relevant high-order nonlinear effect is that of self-steepening (SS), which is responsible for the optical shock of short pulses [7]. However, in the case of soliton propagation no optical shock occurs due to self-steepening [8], but pulses experience a time shift that adds to that produced by the RIFS. Self-steepening is modeled by introducing the parameter s in a first order expansion of the nonlinear coefficient in the frequency domain as $\gamma(\Omega) = \gamma_0\,(1+s\frac{\Omega}{\omega_0})$, where ω_0 is the pulse central frequency, and $\Omega = \omega - \omega_0$ is the frequency detuning from ω_0 [7]. It is worth mentioning that SS plays a pivotal role in nonlinear processes involving large bandwidths, such as in supercontinuum generation [9], [10].

Propagation of light pulses in optical fibers is customarily modeled by the generalized nonlinear Schrödinger equation (GNLSE) [7]. However, a severe drawback of the GNLSE is that it does not conserve the number of photons in lossless waveguides unless the self-steepening parameter is set to $s = 1$ [11]. This fact renders the GNLSE inadequate when applied to waveguides with an arbitrary frequency dependence of the nonlinear coefficient. This, in turn, has motivated the introduction of alternative modeling approaches [12]–[14]. In this paper, we resort to the photon-conserving generalized nonlinear Schrödinger equation (pcGNLSE) [15]. The pcGNLSE, which reduces to the GNLSE whenever $s = 1$, reads

$$\frac{\partial \tilde{A}_\omega}{\partial z} = i\beta(\omega)\tilde{A}_\omega + i\frac{\overline{\gamma}(\omega)}{2}\mathcal{F}\left(C^* B^2\right) + i\frac{\overline{\gamma}^*(\omega)}{2}\mathcal{F}\left(B^* C^2\right) + if_{\mathrm{R}}\overline{\gamma}^*(\omega)\mathcal{F}\left(B\int_0^\infty h_{\mathrm{R}}(\tau)|B(t-\tau)|^2 d\tau - B|B|^2\right), \quad (1)$$

where $\overline{\gamma}(\omega) = \omega\tilde{r}$, $\tilde{B} = \tilde{r}\tilde{A}$, $\tilde{C} = \tilde{r}^*\tilde{A}$, and $\tilde{r} = \sqrt[4]{\gamma(\omega)/\omega}$; $h_{\mathrm{R}}(t)$ models the delayed Raman response and f_{R} is the fractional Raman contribution to the nonlinearity. Most remarkably, this equation can be solved with the very same numerical methods as the GNLSE, e.g., the split-step Fourier algorithm [16].

The focus of this paper is on an original proposal of a simple measurement scheme of the self-steepening parameter, s, and the fractional Raman contribution, f_{R}.

Nicolás Linale, Juan Bonetti, and Diego F. Grosz are with the Depto. de Ingeniería en Telecomunicaciones, Centro Atómico Bariloche, GDTyPE, GAIyANN, Comisión Nacional de Energía Atómica, Río Negro 8400, Argentina, and with Consejo Nacional de Investigaciones Científicas y Técnicas (CONICET), Ciudad Autónoma de Buenos Aires 1425, Argentina.

Pablo I. Fierens is with the Centro de Optoelectrónica, Instituto Tecnológico de Buenos Aires (ITBA), Ciudad Autónoma de Buenos Aires 1106, Argentina, and with Consejo Nacional de Investigaciones Científicas y Técnicas (CONICET), Ciudad Autónoma de Buenos Aires 1425, Argentina.

Santiago M. Hernandez, is with Instituto Balseiro, Universidad Nacional de Cuyo, Río Negro 8400, Argentina.

It is important to emphasize that although these parameters are of utmost relevance when modeling short-pulse nonlinear propagation in optical fibers, they are commonly either assumed or computed from analytical models.

The remaining of this paper is organized as follows: Section II briefly reviews some other measurement techniques found in the literature. Section III presents the proposed scheme and makes a detailed comparison with another recently introduced measurement procedure. Finally, Section IV closes the paper with some final remarks and conclusions.

II. A BRIEF REVIEW OF MEASUREMENT TECHNIQUES

Several ways of estimating the fractional Raman contribution have been proposed in the literature. Hellwarth et al. [17] resort to measurements of intensity-induced polarization changes and the Raman differential scattering cross section to determine $h_{\rm R}(t)$ and $f_{\rm R}$ for several glasses. In the seminal work of Stolen and colleagues [18], [19] a relation between the Raman gain and the differential scattering cross section is used for fused silica, and $f_{\rm R}$ can be calculated from the independent measurement of both quantities.

The Raman gain spectrum is related to the Fourier transform of $h_R(t)$, the fractional Raman contribution, and the nonlinear refractive index of the material. Thus, if the Raman response $h_R(t)$ is known, independent measurements of the Raman gain and the nonlinear refractive index make possible the estimation of $f_{\rm R}$ [20], [21]. However, precise measurements of those quantities are difficult, impeding accurate estimations of the fractional Raman contribution [22]. Finally, $f_{\rm R}$ is sometimes estimated by fitting measured pulse spectra to simulations [23].

We also have proposed an alternative method to measure $f_{\rm R}$ in Ref. [24] based on results obtained with the GNLSE and thus only valid for $s = 1$. It is worth mentioning the underlying idea of this previous proposal as it is related to our present work. Studying the modulation instability (MI) phenomenon, Shukla and Rasmussen [25] and De Angelis et al. [26] showed that, in the absence of Raman scattering, the MI gain disappears if the pump power is greater than a given cutoff power (COP) (see, also, Ref. [27]), a fact often overlooked in the literature. However, when the effect of Raman is accounted for there still exists gain beyond the COP. Moreover, when the pump power exceeds the cutoff power, the MI gain spectral profile follows the Raman spectrum, but with a peak-gain frequency that depends both on the pump power and the fractional Raman contribution [28], [29]. This observation allows for the estimation of $f_{\rm R}$ through the measurement of the MI-gain peak frequency [24]. We shall henceforth refer to this situation as the *Raman-dominated gain* (RDG). Further, the analysis of the MI gain and the COP in the absence of Raman scattering has been extended for arbitrary frequency dependent nonlinear coefficients in Refs. [30], [31]. In particular, in Ref. [31], two distinct modulation instability regimes were observed depending upon the SS parameter: Ultra-wideband and narrowband MI gain.

Notwithstanding its relevance, there is not much work in the literature on the direct measurement of the SS parameter. Since s is related to the effective area of the fiber [11], most of the work has focused either on the numerical estimation [9], [32], [33] or the measurement of the latter [34], [35]. It must be emphasized, however, that the self-steepening parameter is determined not only by the frequency dependence of the mode effective area, but also by the frequency dependence of the nonlinear refractive index (see, e.g., [36], [37]). Moreover, s can differ significantly from unity [9], [36]–[39], the photon-conserving value under the GNLSE which is oftentimes assumed in the literature.

We have recently put forth a pulsed measurement scheme of the SS parameter, relying on the time delay experienced by solitons upon propagation but neglecting the influence of Raman scattering [40]. In the presence of Raman scattering, however, the time delay experienced by the soliton depends on both the SS parameter and Raman. As it was shown in Ref. [2], for relatively long solitons (> 100 fs), the frequency (Ω_p) and time (q_p) shifts are given by

$$\Omega_p(z) = -\frac{8T_{\rm R}\gamma_0 P_0}{15T_0^2}z, \qquad q_p(z) = \frac{\beta_2\Omega_p}{2}z + \frac{(s+2)\gamma_0 P_0}{3\omega_0}z, \tag{2}$$

where β_2 is the GVD parameter, $\gamma_0 = \gamma(0)$, P_0 and T_0 are the soliton peak power and the $1/e$-half width, respectively, and $T_{\rm R}$ is the effective Raman parameter [7]. These expressions were derived neglecting higher-order dispersion terms and for pulses satisfying the fundamental soliton condition, i.e., $T_0^2\gamma_0 P_0/\beta_2 = 1$. The linear relation between the time shift q_p and s in Eq. 2 suggests a direct way for the measurement of the self-steepening parameter. Although $f_{\rm R}$ can also be obtained by measuring the frequency shift, and with knowledge of the Raman response $h_{\rm R}(t)$, this was not reported in Ref. [40]. We shall henceforth refer to the scheme that allows for the measurement of both the SS parameter and the fractional Raman contribution from Eqs. 2 as the *pulsed method*. Even though this pulsed method is direct and simple, it might not always be possible to find the right soliton sources for the spectral range of interest. Moreover, as the time shift due to Raman scattering is larger than that from self-steepening, a small error in the measurement of the frequency shift may lead to large errors in the estimation of s, strongly limiting the applicability of the pulsed method. Furthermore, the required propagation distance might be inconveniently long if pulses lie close to zero-dispersion wavelength (ZDW) of the waveguide.

III. CW MEASUREMENT METHOD

In this work we focus on an original proposal that allows for the simultaneous measurement of both s and f_{R}, based on a simple spectral measurement of the modulation instability gain under the RDG condition, which we shall henceforth refer to as the *CW method*. The MI gain, g_{MI}, can be derived by departing from a linear stability analysis of the pcGNLSE (see e.g. [7], [41]). Although an expression for g_{MI} is needed for a characterization of the modulation instability phenomenon, it is not required to understand the proposed measurement scheme and, thus, we refer the interested reader to Appendix A for its full derivation. Figure 1 shows an example of the MI gain for a chalcogenide fiber with $\beta_2 = -10^{-4}$ ps^2/ m, $\gamma_0 = 1$ W^{-1} m^{-1} [42], [43], $s = 1.2$, and $f_{\mathrm{R}} = 0.1$, as predicted by the pcGNLSE. The Raman response is modeled as $h_{\mathrm{R}}(t) = (\tau_1^{-2} + \tau_2^{-2})\tau_1 \exp(-t/\tau_2)\sin(-t/\tau_1)$, where $\tau_1 = 15.5$ fs and $\tau_2 = 230.5$ fs [23], [44], and the pump wavelength is $\lambda_0 = 5000$ nm. The top panel shows the MI gain under the RDG regime with a pump power of $P_0 = 20$ W, and red dots mark MI-gain maxima. The bottom panel shows g_{MI} as a function of power and frequency. The blue dashed line marks the cutoff power and thus the limit of the RDG.

The dependence of the RDG peak frequency with the fractional Raman contribution in the framework of the GNLSE was already shown in Ref. [24]. Here, we extend this result with a modulation instability analysis of the pcGNLSE, and thus valid for any arbitrary SS parameter. The derivation of the MI gain in this setting reveals that $g_{\mathrm{MI}} = g_{\mathrm{MI}}(\Omega, P_0, f_{\mathrm{R}}, s)$, i.e., it not only depends on the input power and frequency (see bottom panel in Fig. 1) but also on the fractional Raman contribution and the self-steepening parameter. This is put in evidence in Fig. 2 which shows the MI gain vs. s (top panel) and f_{R} (bottom panel).

The dependence of g_{MI} on f_{R} and s suggests that these parameters can be estimated from gain measurements. Furthermore, the distinctiveness of MI gain peaks in the top panel of Fig. 1 suggests that simple measurements of these peaks can be advantageously used for such an estimation. Indeed, let us fix a pump power P_0 larger than the COP and define the gain and position of one of the RDG peaks as

$$g_{\mathrm{MAX}}(f_{\mathrm{R}}, s) = \max_{\Omega>0} g_{\mathrm{MI}}(\Omega, P_0, f_{\mathrm{R}}, s), \tag{3}$$

$$\Omega_{\mathrm{MAX}}(f_{\mathrm{R}}, s) = \arg\max_{\Omega>0} g_{\mathrm{MI}}(\Omega, P_0, f_{\mathrm{R}}, s). \tag{4}$$

These functions can be easily computed from the analytical expression of the MI gain (see Appendix A). Let us call $\overline{g}$, $\overline{\Omega}$ the actual measurements of the peak gain and position, respectively. Then, the fractional Raman contribution and the SS parameter can be estimated by solving the two equations $g_{\mathrm{MAX}}(f_{\mathrm{R}}, s) = \overline{g}$ and $\Omega_{\mathrm{MAX}}(f_{\mathrm{R}}, s) = \overline{\Omega}$. Geometrically, the estimation corresponds to the intersection of two independent curves in the (f_{R}, s)-plane (see Fig. 3)

$$g_{\mathrm{MAX}}(f_{\mathrm{R}}, s) - \overline{g} = 0, \qquad \Omega_{\mathrm{MAX}}(f_{\mathrm{R}}, s) - \overline{\Omega} = 0. \tag{5}$$

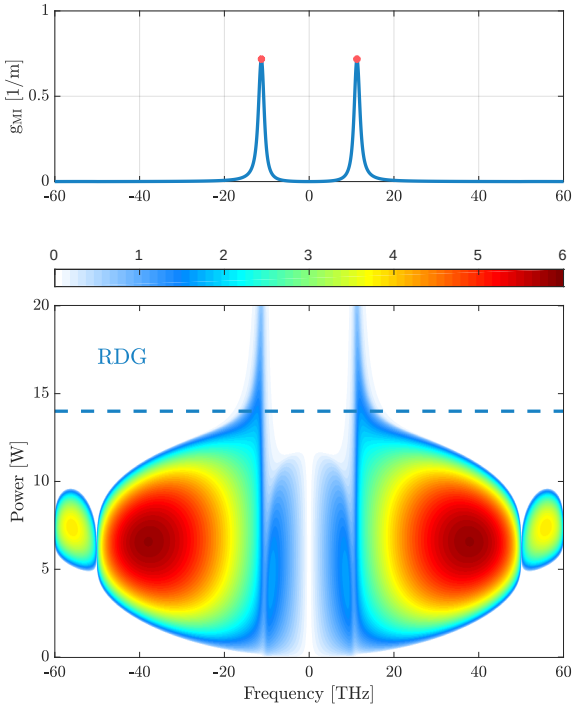

Fig. 1: (Top panel) Raman-dominated gain for a pump power $P_0 = 20$ W. Red dots mark gain maxima. (Bottom panel) MI gain for a chalcogenide fiber vs. pump power and frequency. The dashed line marks the cutoff power.

In Fig. 3 we explore the proposed scheme by means of two simulated examples and we compare results with those obtained with the pulsed method (see Section II). The top panel shows results for a waveguide in the mid IR. Fiber parameters are the same as in Fig. 1, except for $\beta_2 = -0.1$ ps^2/ km. The self-steepening parameter and fractional Raman contribution are set to 2 and 0.25, respectively (marked with a red star in the figure). For the CW method we launch a 100-W CW laser (with a realistic 60-dB signal-to-noise ratio) at 5000 nm. The blue dashed line shows the dependence of Ω_{MAX} and the green solid line shows that of g_{MAX}, and the intersection of both curves corresponds to the estimated values of f_{R} and s (black square). As it can be seen, the estimation is in excellent agreement with the expected values. For reference, we show the estimation employing the pulsed method (black triangle). This is done by launching a 200-fs fundamental soliton along $50L_{\mathrm{D}}$, with L_{D} the dispersion length defined by $L_{\mathrm{D}} = T_0^2/|\beta_2|$, and f_{R} and s are obtained from Eqs. 2 and the measurement of the

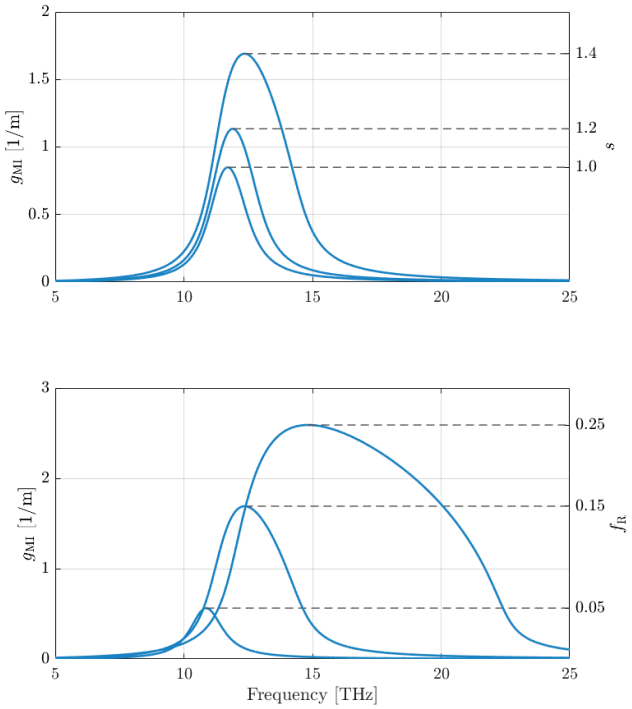

Fig. 2: Raman-dominated gain for different values of (top) s ($f_{\rm R} = 0.15$) and (bottom) $f_{\rm R}$ ($s = 1$), and for the same parameters used in Fig. 1.

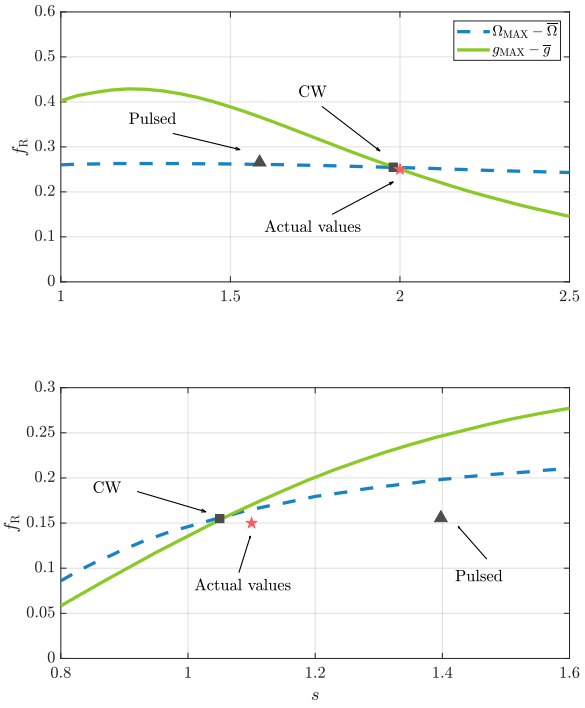

Fig. 3: Application of the CW (black square) and pulsed methods (black triangle) in the mid IR (top) and near IR (bottom). Red stars mark the actual values of $f_{\rm R}$ and s. The estimation of the CW scheme is given by the intersection of the curves for the MI-gain peak (green-dotted line) and its frequency (blue dashed line).

Parameter	Fig. 3 (top)	Fig. 3 (bottom)
Spectral range	Mid IR	Near IR
Optical fiber	Chalcogenide	PCF
λ_0 [nm]	5000	800
s	2.0	1.1
$f_{\rm R}$	0.25	0.15
β_2 [ps^2/ km]	$-0.1^{(a)}$	$-0.1^{(a)}$
γ_0 [W^{-1} km^{-1}]	1000	130
CW method		
P_0 [W]	$100^{(b)}$	$6000^{(b)}$
Pulsed method		
P_0 [mW]	2.5	20
T_0 [ps]	0.2	0.2

TABLE I: Summary of simulation parameters for the two spectral bands. (a) The pump wavelength is assumed to lie close to the zero-dispersion wavelength (ZDW). (b) A realistic 60-dB signal-to-noise ratio was assumed.

frequency and time shifts. Note that although higher-order dispersion was neglected in these simulations, it can be readily incorporated into the model for both the CW (see Ref. [30]) and pulsed schemes (see Ref. [40]). For the sake of clarity, simulation parameters used in Fig. 3 are summarized in Table I.

As it was mentioned, the reason for the poorer performance of the pulsed method is that, since the Raman contribution to the temporal shift is larger than that from self-steepening, a small error in the measurement of the frequency shift leads to a large error in the estimation of the SS parameter. In numerical simulations this error is given by the frequency discretization, which in results shown in Fig. 3 was set to coincide with the typical resolution of a spectrum analyzer in order to replicate real experimental conditions. Indeed, observe that while the error in the estimation of $f_{\rm R}$ is only 5.6 %, it is as high as 27 % for the self-steepening parameter.

The bottom panel in Fig. 3 shows the application of the CW method in the near IR. Fiber parameters are comparable to those of a photonic-crystal fiber (PCF), i.e. $\beta_2 = -0.1$ ps^2/ km and $\gamma_0 = 130$ W^{-1} km^{-1}. The self-steepening parameter and fractional Raman contribution are set to 1.1 and 0.15, respectively (marked with a red star). For the CW method we launch a 6000-W CW laser (60 dB SNR) at 800 nm, close to the ZDW of the PCF. For the pulsed method, we launch a 200-fs fundamental soliton along $10L_{\rm D}$. Once again, we observe a very good agreement between the CW method (black square) and the actual values (red star), and a poorer performance of the pulsed method (black triangle). It is instructive

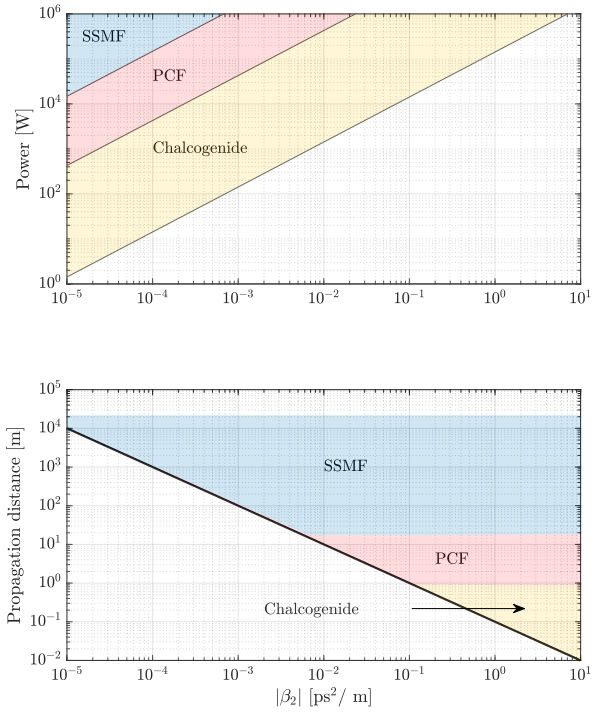

Fig. 4: Limitations of the CW and pulsed methods. (Top) Pump power required for the CW method and (bottom) propagation distance required for the pulsed method. (Top) Diagonal lines show the approximate cutoff power for each spectral band and each fiber type. (Bottom) The top of each colored band is given by the corresponding effective attenuation length. In both panels, colored regions indicate the parameter range for practical application of each method.

to analyze the accuracy of the CW scheme in terms of experimental errors. For instance, assuming a typical instrument resolution at 800 nm of ~ 1 mW and ~ 0.2 nm, a standard error analysis yields and uncertainty of $\sim 7\%$ and $\sim\ 9\%$ in the fractional Raman contribution and the SS parameter, respectively, in agreement with values found in the literature (see, e.g., Ref. [22]).

It is relevant to point out that the CW method can be realized with quasi-CW pulsed laser sources, i.e., whenever the bandwidth of the modulated pump represents a small fraction of the Raman peak frequency of the medium, as this allows to attain large peak powers with modest average powers that may otherwise damage the waveguide under test. As it turns out, this condition is not overly restrictive. As an example, the Raman gain peak in silica lies $\approx\ 13$ THz from the pump laser [7]; as such, modulated lasers producing pulses longer than 100 ps can be regarded as quasi-CW sources (see, e.g., Ref. [45].)

Some limitations hinder the application of both the CW and pulsed schemes. The power required to operate in the RDG regime in the CW method might be too large when the pump frequency lies far from the ZDW, as the cutoff power is approximately given by $P_{\rm co} \approx \omega_0^2|\beta_2|/\gamma_0 s$ (see Ref. [27]). This is depicted in the top panel of Fig. 4 for $s = 1$, and for different wavelengths and common fibers, whose characteristic parameters are summarized in Table II. Black solid lines indicate the limit of application of the CW method for each fiber. In the case of the pulsed method, the propagation distance may be too long if the pump wavelength lies close to the ZDW, as the required distance must be in the order of $L_{\rm pulsed} \approx 10T_0^2/\beta_2$ [40]. The dependence of $L_{\rm pulsed}$ with the GVD parameter β_2 is shown in the bottom panel of Fig. 4. The upper limit for each band indicates the respective fiber effective length due to attenuation. Observe that whenever the pump wavelength is away from the ZDW, i.e., for large values of β_2, the pulsed method appears to be more suitable than the CW scheme. However, when the pump wavelength is closer to the ZDW one may consider using the CW method.

Regarding available laser sources, there is a lack of short-pulse sources in the mid IR, a region where the CW method is more appropriate due to the highly nonlinear (e.g., chalcogenide) fibers available and typical values of the ZDW. In the near IR, particularly in the telecommunication window at 1.5 µm, the fiber nonlinearity is relatively small and, for most cases, the ZDW does not lie within this spectral band. However, short-pulse sources are readily available in this spectral region and thus the pulsed method is more appropriate.

There is another limitation for the CW scheme proposed in this paper. Indeed, there is no MI cutoff power for large values of the fractional Raman contribution and the self-steepening parameter. However, it can be shown that this is not the case for values commonly found in the literature, that is, $f_{\rm R}$ between $0.1 - 0.3$ [3], [19], [23], [47] and s between $1 - 2.5$ [9], [38], [39].

IV. Conclusions

We find in the literature that the fractional Raman contribution and the self-steepening are two relevant parameters in fiber optics which are oftentimes either assumed or computed from analytical models. In this sense, we believe that there is a lack of simple and direct measurement procedures for these two relevant parameters and our proposal intends to fill this gap. Indeed, we showed that a simple measurement can provide accurate estimations of both values.

Our proposal is based on an original modulation instability analysis of the photon-conserving generalized nonlinear Schrödinger equation (pcGNLSE), which guarantees that it can be applied to media with arbitrary frequency-dependent nonlinear coefficients. Moreover, the scheme requires only the CW or quasi-CW pumping of the waveguide under test and a few simple spectral

TABLE II: Parameters of fibers used in Fig. 4

Fiber	Wavelength [μm]	Attenuation [dB/m]	ZNW [μm]	Nonlinear coeff. [W^{-1} m^{-1}]
PCF	0.80	0.25	0.77 - 0.80	0.13
SSMF	1.55	2×10^{-4}	1.31	10^{-3}
Chalcogenide[(a)]	5.00	0.80 - 5.00	3.00 - 5.00	1.00

[(a)]Parameters taken from Refs. [42], [43], [46].

measurements. Finally, we discussed the practical limitations of our proposal, provided a detailed analysis of its application to different spectral ranges of interest, and compared results to a recently introduced pulsed method.

ACKNOWLEDGMENTS

Fruitful discussions with A. D. Sánchez are gratefully acknowledged.

APPENDIX A
MODULATION INSTABILITY

In this Appendix we provide the derivation of the modulation instability (MI) gain departing from a linear stability analysis of the photon-conserving generalized nonlinear Schrödinger equation (pcGNLSE).

We start by considering the photon-conserving generalized equation (pcGNLSE) introduced in Ref. [15],

$$\frac{\partial \tilde{A}_\omega}{\partial z} = i\beta(\omega)\tilde{A}_\omega + i\frac{\omega\tilde{r}(\omega)}{2}\mathcal{F}\left(C^*B^2\right) + i\frac{\omega\tilde{r}^*(\omega)}{2}\mathcal{F}\left(B^*C^2\right) + if_{\mathrm{R}}\omega\tilde{r}^*(\omega)\mathcal{F}\left(B\int_0^\infty h_{\mathrm{R}}(\tau)|B(t-\tau)|^2d\tau - B|B|^2\right), \quad (6)$$

where z is the propagation axis, $\tilde{A}_\omega$ is the Fourier transform of the complex envelope A, $\beta(\omega)$ is the fiber dispersion profile, f_{R} is the fractional Raman contribution, and $h_{\mathrm{R}}(t)$ is the delayed nonlinear response. The fields B and C are defined in the frequency domain as $\tilde{B}_\omega = \tilde{r}(\omega)\tilde{A}_\omega$ and $\tilde{C}_\omega = \tilde{r}^*(\omega)\tilde{A}_\omega$, respectively, where $\tilde{r}(\omega) = \sqrt[4]{\gamma(\omega)/\omega}$ and $\gamma(\omega)$ is the fiber nonlinear profile. As usual in modulation instability analysis [7], [41], we put forth the ansatz

$$A(z,t) = \sqrt{P_0}e^{ik_pz - i\omega_0t} + a(z,t), \quad (7)$$

where P_0, ω_0, and k_p are the power, frequency, and wavenumber, respectively, of the stationary solution to Eq. 6, and $a(z,t)$ is a small perturbation, assumed to satisfy $|a(z,t)|^2 \ll P_0$. For convenience, we write the perturbation as

$$a(z,t) = \int_{-\infty}^{\infty} a_s(z,\Omega)e^{ik(\Omega)z - i(\omega_0+\Omega)t}\,d\Omega. \quad (8)$$

By replacing Eq. 7 into Eq. 6, and taking into account only first-order terms of a_s, we obtain the system of differential equations

$$\begin{cases} \partial_z a_s(z,\Omega) = i\kappa(\Omega)a_s^*(z,-\Omega)e^{i\Delta kz} \\ \partial_z a_s(z,-\Omega) = i\kappa(-\Omega)a_s^*(z,\Omega)e^{i\Delta k^*z}, \end{cases} \quad (9)$$

where

$$\begin{cases} \kappa(\Omega) = (\omega_0+\Omega)P\left(\mathrm{Re}\left[\tilde{r}_s\tilde{r}_i\tilde{r}_p^2\right] + f_{\mathrm{R}}\tilde{r}_s^*\tilde{r}_i^*\tilde{r}_p^2\left(\tilde{h}_{\mathrm{R}}(-\Omega)-1\right)\right) \\ \Delta k = 2k_p - k_s - k_i^* \end{cases} \quad (10)$$

and we use the notation $\tilde{r}_i = \tilde{r}(\omega_0-\Omega)$, $k_s = k(\Omega)$, and $k_i = k(-\Omega)$, according to the usual definition of *signal* and *idler* in parametric processes. The solution of Eq. 9 is

$$a_s(z,\Omega) = a_s^+\exp\left(-i\frac{\Delta k}{2}z + i\sqrt{\left(\frac{\Delta k}{2}\right)^2 - \kappa_s\kappa_i^*}z\right) + a_s^-\exp\left(-i\frac{\Delta k}{2}z - i\sqrt{\left(\frac{\Delta k}{2}\right)^2 - \kappa_s\kappa_i^*}z\right), \quad (11)$$

where $\kappa_s = \kappa(\Omega)$, $\kappa_i = \kappa(-\Omega)$ and

$$\begin{cases} a_s^+ = \left[(\Lambda + \Delta k/2)a_s(0,\Omega) - \kappa_s a_s^*(0,-\Omega)\right]/2\Lambda \\ a_s^- = \left[(\Lambda - \Delta k/2)a_s(0,\Omega) + \kappa_s a_s^*(0,-\Omega)\right]/2\Lambda \\ \Lambda = \sqrt{(\Delta k/2)^2 - \kappa_s\kappa_i^*}. \end{cases} \quad (12)$$

Although Eq. 11 provides a complete description of the spectral evolution, a simpler approach is commonly used in the study of the modulation instability process, whereby the growth of MI sidebands is given by

$$|a_s(z,\Omega)|^2 \propto \exp(g_{\mathrm{MI}}(\Omega)z), \quad (13)$$

where

$$g_{\mathrm{MI}}(\Omega) = \max\left(2\mathrm{Im}\left[\frac{\Delta k}{2} \pm \sqrt{\left(\frac{\Delta k}{2}\right)^2 - \kappa_s\kappa_i^*}\right]\right) \quad (14)$$

is the *MI gain*, i.e., the dominant exponential at long propagation distances.

APPENDIX B
STANDARD ERROR ANALYSIS

In this Appendix we calculate uncertainties in the proposed CW method. By standard analysis, errors incurred in obtaining Δf_{R} and Δs are given by

$$\begin{bmatrix} \Delta f_{\mathrm{R}} \\ \Delta s \end{bmatrix} = \mathbf{J}^{-1}\begin{bmatrix} \Delta g \\ \Delta\Omega \end{bmatrix}, \quad (15)$$

$$\mathbf{J} = \begin{bmatrix} \frac{\partial}{\partial f_{\mathrm{R}}} g_{\mathrm{MAX}}(f_{\mathrm{R}}, s) & \frac{\partial}{\partial s} g_{\mathrm{MAX}}(f_{\mathrm{R}}, s) \\ \\ \frac{\partial}{\partial f_{\mathrm{R}}} \Omega_{\mathrm{MAX}}(f_{\mathrm{R}}, s) & \frac{\partial}{\partial s} \Omega_{\mathrm{MAX}}(f_{\mathrm{R}}, s) \end{bmatrix}, \quad (16)$$

where $\mathbf{J}$ is the Jacobian matrix, g_{MAX} and Ω_{MAX} are the peak gain and its frequency position, respectively, as obtained from any one of the measured MI gain peaks, and Δg and $\Delta\Omega$ stand for the the uncertainty in these magnitudes as given by the resolution of the measuring device. Assuming realistic power and frequency resolutions of 1 mW and 0.2 nm, respectively, the estimated uncertainties are found to be ~ 7 % and ~ 9 % for the fractional Raman contribution and for the SS parameter, respectively.

REFERENCES

[1] G. P. Agrawal, "Effect of intrapulse stimulated Raman scattering on soliton-effect pulse compression in optical fibers," *Optics Letters*, vol. 15, no. 4, pp. 224–226, 1990.

[2] N. Linale, P. I. Fierens, and D. F. Grosz, "Probing higher-order nonlinearities with ultrashort solitons," in *Frontiers in Optics*, vol. To be published. Optical Society of America, 2020.

[3] Q. Lin and G. P. Agrawal, "Raman response function for silica fibers," *Optics Letters*, vol. 31, no. 21, pp. 3086–3088, 2006.

[4] B. R. Washburn, S. E. Ralph, P. A. Lacourt, J. M. Dudley, W. T. Rhodes, R. S. Windeler, and S. Coen, "Tunable near-infrared femtosecond soliton generation in photonic crystal fibres," *Electronics Letters*, vol. 37, no. 25, pp. 1510–1512, 2001.

[5] M. E. Masip, A. A. Rieznik, P. G. König, D. F. Grosz, A. V. Bragas, and O. E. Martinez, "Femtosecond soliton source with fast and broad spectral tunability," *Optics Letters*, vol. 34, no. 6, pp. 842–844, 2009.

[6] J. H. Lee, J. van Howe, C. Xu, and X. Liu, "Soliton self-frequency shift: experimental demonstrations and applications," *IEEE Journal of Selected Topics in Quantum Electronics*, vol. 14, no. 3, pp. 713–723, 2008.

[7] G. P. Agrawal, *Nonlinear Fiber Optics*. Academic Press, 2013.

[8] K. Ohkuma, Y. H. Ichikawa, and Y. Abe, "Soliton propagation along optical fibers," *Optics Letters*, vol. 12, no. 7, pp. 516–518, 1987.

[9] B. Kibler, J. M. Dudley, and S. Coen, "Supercontinuum generation and nonlinear pulse propagation in photonic crystal fiber: influence of the frequency-dependent effective mode area," *Applied Physics B*, vol. 81, no. 2-3, pp. 337–342, 2005.

[10] B. Barviau, B. Kibler, and A. Picozzi, "Wave-turbulence approach of supercontinuum generation: Influence of self-steepening and higher-order dispersion," *Physical Review A*, vol. 79, no. 6, p. 063840, 2009.

[11] K. Blow and D. Wood, "Theoretical description of transient stimulated Raman scattering in optical fibers," *IEEE Journal of Quantum Electronics*, vol. 25, no. 12, pp. 2665–2673, Dec. 1989.

[12] S. Wen, Y. Xiang, X. Dai, Z. Tang, W. Su, and D. Fan, "Theoretical models for ultrashort electromagnetic pulse propagation in nonlinear metamaterials," *Physical Review A*, vol. 75, no. 3, p. 033815, 2007.

[13] J. Lægsgaard, "Mode profile dispersion in the generalized nonlinear schrödinger equation," *Optics Express*, vol. 15, no. 24, pp. 16 110–16 123, 2007.

[14] O. Vanvincq, J. C. Travers, and A. Kudlinski, "Conservation of the photon number in the generalized nonlinear Schrödinger equation in axially varying optical fibers," *Physical Review A*, vol. 84, p. 063820, Dec 2011.

[15] J. Bonetti, N. Linale, A. D. Sánchez, S. M. Hernandez, P. I. Fierens, and D. F. Grosz, "Photon-conserving generalized nonlinear Schrödinger equation for frequency-dependent nonlinearities," *Journal of the Optical Society of America B*, vol. 37, no. 2, pp. 445–450, 2020.

[16] J. Hult, "A fourth-order Runge–Kutta in the interaction picture method for simulating supercontinuum generation in optical fibers," *Journal of Lightwave Technology*, vol. 25, no. 12, pp. 3770–3775, 2007.

[17] R. Hellwarth, J. Cherlow, and T.-T. Yang, "Origin and frequency dependence of nonlinear optical susceptibilities of glasses," *Physical Review B*, vol. 11, no. 2, p. 964, 1975.

[18] R. H. Stolen and E. P. Ippen, "Raman gain in glass optical waveguides," *Applied Physics Letters*, vol. 22, no. 6, pp. 276–278, 1973.

[19] R. H. Stolen, J. P. Gordon, W. Tomlinson, and H. A. Haus, "Raman response function of silica-core fibers," *Journal of the Optical Society of America B*, vol. 6, no. 6, pp. 1159–1166, 1989.

[20] J. Hu, C. R. Menyuk, L. B. Shaw, J. S. Sanghera, and I. D. Aggarwal, "Raman response function and supercontinuum generation in chalcogenide fiber," in *Conference on Lasers and Electro-Optics/Quantum Electronics and Laser Science Conference and Photonic Applications Systems Technologies*. Optical Society of America, 2008, pp. 1–2.

[21] J. Hu, C.Menyuk, L. B. Shaw, J. S. Sanghera, and I. D. Aggarwal, "Maximizing the bandwidth of supercontinuum generation in As_2Se_3 chalcogenide fibers," *Optics Express*, vol. 18, no. 7, p. 6722, mar 2010.

[22] R. E. Slusher, G. Lenz, J. Hodelin, J. Sanghera, L. B. Shaw, and I. D. Aggarwal, "Large Raman gain and nonlinear phase shifts in high-purity as2se3 chalcogenide fibers," *Journal of the Optical Society of America B*, vol. 21, no. 6, pp. 1146–1155, Jun 2004.

[23] C. Xiong, E. Magi, F. Luan, A. Tuniz, S. Dekker, J. S. Sanghera, L. B. Shaw, I. Aggarwal, and B. J. Eggleton, "Characterization of picosecond pulse nonlinear propagation in chalcogenide As2S3 fiber," *Applied Optics*, vol. 48, no. 29, pp. 5467–5474, 2009.

[24] A. D. Sánchez, N. Linale, J. Bonetti, S. M. Hernandez, P. I. Fierens, G. Brambilla, and D. F. Grosz, "Simple method for estimating the fractional Raman contribution," *Optics Letters*, vol. 44, no. 3, pp. 538–541, 2019.

[25] P. K. Shukla and J. J. Rasmussen, "Modulational instability of short pulses in long optical fibers," *Optics Letters*, vol. 11, no. 3, pp. 171–173, 1986.

[26] C. D. Angelis, G. Nalesso, and M. Santagiustina, "Role of nonlinear dispersion in the dynamics of induced modulational instability in Kerr media," *Journal of the Optical Society of America B*, vol. 13, no. 5, pp. 848–855, May 1996.

[27] S. M. Hernandez, P. I. Fierens, J. Bonetti, A. D. Sánchez, and D. F. Grosz, "A geometrical view of scalar modulation instability in optical fibers," *IEEE Photonics Journal*, vol. 9, no. 5, pp. 1–8, 2017.

[28] A. D. Sánchez, S. M. Hernandez, J. Bonetti, P. I. Fierens, and D. F. Grosz, "Tunable Raman gain in mid-IR waveguides," *Journal of the Optical Society of America B*, vol. 35, no. 1, pp. 95–99, 2018.

[29] A. D. Sánchez, P. I. Fierens, S. M. Hernandez, J. Bonetti, G. Brambilla, and D. Grosz, "Anti-Stokes Raman gain enabled by modulation instability in mid-ir waveguides," *Journal of the Optical Society of America B*, vol. 35, no. 11, pp. 2828–2832, 2018.

[30] N. Linale, J. Bonetti, A. D. Sánchez, S. Hernandez, P. I. Fierens, and D. F. Grosz, "Modulation instability in waveguides with an arbitrary frequency-dependent nonlinear coefficient," *Optics Letters*, vol. 45, no. 9, pp. 2498–2501, 2020.

[31] N. Linale, P. Fierens, S. Hernandez, J. Bonetti, and D. Grosz, "Narrowband and ultra-wideband modulation instability in nonlinear metamaterial waveguides," *JOSA B*, vol. 37, no. 11, pp. 3194–3199, 2020.

[32] G. Chang, T. B. Norris, and H. G. Winful, "Optimization of supercontinuum generation in photonic crystal fibers for pulse compression," *Optics Letters*, vol. 28, no. 7, pp. 546–548, 2003.

[33] S. Chugh, A. Gulistan, S. Ghosh, and B. Rahman, "Machine learning approach for computing optical properties of a photonic crystal fiber," *Optics Express*, vol. 27, no. 25, pp. 36 414–36 425, 2019.

[34] W. S. Wong, X. Peng, J. M. McLaughlin, and L. Dong, "Breaking the limit of maximum effective area for robust single-mode propagation in optical fibers," *Optics Letters*, vol. 30, no. 21, pp. 2855–2857, 2005.

[35] M. C. P. Huy, A. Baron, S. Lebrun, R. Frey, and P. Delaye, "Characterization of self-phase modulation in liquid filled hollow core photonic band gap fibers: erratum," *Journal of the Optical Society of America B*, vol. 30, no. 6, pp. 1651–1651, 2013.

[36] N. C. Panoiu, X. Liu, and R. M. Osgood, "Nonlinear dispersion in silicon photonic wires," in *2008 Conference on Lasers and Electro-Optics and 2008 Conference on Quantum Electronics and Laser Science*. IEEE, 2008, pp. 1–2.

[37] N. C. Panoiu, X. Liu, and R. M. Osgood Jr, "Self-steepening of ultrashort pulses in silicon photonic nanowires," *Optics Letters*, vol. 34, no. 7, pp. 947–949, 2009.
[38] J. H. Price, T. M. Monro, H. Ebendorff-Heidepriem, F. Poletti, V. Finazzi, J. Y. Leong, P. Petropoulos, J. C. Flanagan, G. Brambilla, X. Feng *et al.*, "Non-silica microstructured optical fibers for mid-ir supercontinuum generation from 2 μm–5 μm," in *Fiber Lasers III: Technology, Systems, and Applications*, vol. 6102. International Society for Optics and Photonics, 2006, p. 61020A.
[39] T. Cheng, W. Gao, X. Xue, T. Suzuki, and Y. Ohishi, "Experimental investigation of multiple Raman peak properties in a hundred-meter tellurite fiber," *Optical Materials Express*, vol. 6, no. 11, pp. 3438–3445, 2016.
[40] N. Linale, P. I. Fierens, J. Bonetti, A. D. Sánchez, S. Hernandez, and D. F. Grosz, "Measuring self-steepening with the photon-conserving nonlinear Schrödinger equation," *Optics Letters*, vol. 45, no. 16, pp. 4535–4538, 2020.
[41] J. Bonetti, S. M. Hernandez, P. I. Fierens, and D. F. Grosz, "Analytical study of coherence in seeded modulation instability," *Physical Review A*, vol. 94, p. 033826, 2016.
[42] B. J. Eggleton, B. Luther-Davies, and K. Richardson, "Chalcogenide photonics," *Nature Photonics*, vol. 5, no. 3, pp. 141–148, 2011.
[43] B. Ung and M. Skorobogatiy, "Chalcogenide microporous fibers for linear and nonlinear applications in the mid-infrared," *Optics Express*, vol. 18, no. 8, pp. 8647–8659, 2010.
[44] N. Granzow, S. P. Stark, M. A. Schmidt, A. S. Tverjanovich, L. Wondraczek, and P. S. J. Russell, "Supercontinuum generation in chalcogenide-silica step-index fibers," *Optics Express*, vol. 19, no. 21, pp. 21 003–21 010, 2011.
[45] K. Tai, A. Hasegawa, and A. Tomita, "Observation of modulational instability in optical fibers," *Physical review letters*, vol. 56, no. 2, p. 135, 1986.
[46] J. S. Sanghera, I. Aggarwal, L. Shaw, C. Floreaa, P. Pureza, V. Nguyen, and F. Kung, "Nonlinear properties of chalcogenide glass fibers," *Journal of Optoelectronics and Advanced Materials*, vol. 8, no. 6, pp. 2148–2155, 2006.
[47] T. S. Saini, A. Kumar, and R. K. Sinha, "Broadband mid-infrared supercontinuum spectra spanning 2–15 μm using As2Se3 chalcogenide glass triangular-core graded-index photonic crystal fiber," *Journal of lightwave technology*, vol. 33, no. 18, pp. 3914–3920, 2015.